Zinc oxide nanoparticle-polymeric thin films for dynamic strain sensing

Kenneth J. Loh · Donghee Chang

Abstract Piezoelectric transducers are becoming increasingly popular for dynamic strain monitoring due to their small form factors and their ability to generate an electrical voltage drop in response to strain. Although numerous types of piezoelectric thin films have been adopted for strain sensing, it has been shown that piezo-ceramics are expensive, brittle, and can fail during operation, while piezo-polymers possess lower piezoelectricity and mechanical stiffness. Thus, the objective of this study is to develop a piezoelectric thin film characterized by high piezoelectricity (i.e., high dynamic strain sensitivities) and favorable mechanical properties (i.e., being conformable to structural surfaces yet stiff). First, zinc oxide (ZnO) nanoparticles are dispersed in polyelectrolyte solutions, and the excess solvent is evaporated for thin film fabrication. The amount of ZnO nanoparticles embedded within the films is varied to yield seven unique sample sets with ZnO weight fractions ranging from 0 to 60%. Upon film fabrication, specimens are mounted in a load frame for monotonic uniaxial testing to explore the films' stress–strain performance and to subsequently determine their mechanical properties (namely, modulus of elasticity, ultimate strength, and ultimate failure strain). Finally, film specimens are also mounted onto cantilevered beams undergoing free vibration due to an applied initial displacement. The generated voltages in response to induced strains in the beams are recorded, and the piezoelectric performance and dynamic strain sensitivities for the different weight fraction films are calculated and compared. Commercial PVDF thin films are also employed in this study for performance comparison.

Introduction

Piezoelectric transducers such as piezo-ceramic lead zirconate titanate (PZT) and poly(vinylidene fluoride) (PVDF) piezo-polymers have been widely adopted for sensing [1], actuation [2], control [3], and energy harvesting [4]. Unique to piezoelectric materials is their inherent ability to simultaneously serve as sensors and actuators. For instance, one can take advantage of the direct piezoelectric effect for dynamic strain sensing and energy harvesting where an electrical potential drop develops in response to an applied strain. The converse is also true, and the piezoelectric transducer can be used as an actuator as it strains due to an applied electric field (i.e., due to the indirect piezoelectric effect) [3, 5]. More importantly, piezoelectric materials are advantageous in that they do not rely on external power sources (e.g., batteries or alternating current (AC) power) for continued operations, unlike strain gages [6], fiber optics [7], wireless sensor nodes [8], microelectromechanical systems (MEMS) devices [9], and other types of sensing systems.

Unfortunately, PZT and PVDF suffer from fundamental limitations intrinsic to their material. Although piezo-ceramic PZT transducers possess high piezoelectricity and d_{33} piezoelectric constants approximately 200–400 pC N^{-1} [10], they are extremely brittle, have high loss factors, and are characterized by highly hysteretic behavior [11]. On the other hand, piezoelectric polymers such as PVDF and

K. J. Loh (✉)
Department of Civil and Environmental Engineering,
University of California, Davis, CA 95616-5294, USA
e-mail: kjloh@ucdavis.edu
URL: http://nesst.engr.ucdavis.edu

D. Chang
Department of Chemical Engineering and Materials Science,
University of California, Davis, CA 95616, USA

PVDF-copolymers are flexible, conformable, and can be fabricated to different sizes and thicknesses [12]. However, they possess considerably lower piezoelectric constants as compared to PZTs (~ 10 pC N^{-1}) and require intricate mechanical stretching to enhance their bulk film piezoelectricity [5, 13]. Furthermore, both PVDF films and PZTs require high-voltage poling so as to enhance their piezoelectricity. Thus, in order to use piezoelectric transducers for sensing applications in complex laboratory and field environments, it is desirable for them to simultaneously possess high piezoelectricity and excellent mechanical properties.

On the other hand, the nanotechnology domain offers a diverse suite of new materials and composite fabrication methodologies for high-performance piezoelectrics [14–16]. Among the plethora of nanomaterials, zinc oxide (ZnO) nanostructures (e.g., nanowires, nanosprings, and nanoparticles, among others) can be readily synthesized and exhibit inherent piezoelectricity [17, 18]. For example, Wang and Song [17] has synthesized aligned ZnO nanowire arrays and has characterized their electrical energy generation via deformation induced by an atomic force microscope tip. Scrymgeour et al. [19] has employed a solution technique for growing ZnO nanorods on silver films, and piezoelectric force microscopy studies estimate that the d_{33} constants of individual nanorods are approximately 4.41 ± 1.73 pm V^{-1}. On the other hand, Lin et al. [20] has fabricated a PZT/ZnO nanowhisker nanocomposite; when compared to monolithic PZT, although the piezoelectric constant of the nanocomposite decreased slightly, the nanocomposite's flexural strength and fracture toughness increased by 40 and 30%, respectively. In general, the aforementioned studies have confirmed the piezoelectric performance of ZnO nanostructures, and it is possible to fabricate piezoelectric ZnO-based structures without the need for high-voltage poling. On the other hand, ZnO nanomaterials have also found diverse applications in polymer solar cells [21] or other nanocomposite systems [22].

The objective of this research is to characterize the mechanical and piezoelectric performance of ZnO nanoparticle-based thin films for dynamic strain monitoring. First, ZnO nanoparticles are dispersed in polyelectrolyte solutions and evaporated in Petri dish molds for film fabrication. A total of seven unique sets of nanocomposites are fabricated, where each set is characterized by a unique nanoparticle weight fraction; the various films are used as is (i.e., without further post-thin film fabrication treatment or high-voltage poling) for the remainder of this study. Second, the as-fabricated films are imaged using scanning electron microscopy (SEM) to evaluate their micro- and nano-scale physical morphology. Then, monotonic uniaxial tensile testing is employed for investigating thin film

mechanical properties. Finally, to evaluate the nanocomposite's piezoelectric performance, the films are also affixed onto cantilevered beam specimens, and their generated voltages are sampled during free vibration response of the beam. The normalized generated voltages are compared to surface strain measurements and PVDF generated voltages, and the relationship between ZnO weight fraction and dynamic strain sensitivity is discussed.

Experimental details

Materials

The raw materials utilized during nanocomposite fabrication are used as is and without further purification or chemical modification. ZnO nanoparticles (20 nm, 99.5% purity) are acquired from Nano Amor, Inc. Polymer powders, namely, poly(sodium 4-styrenesulfonate) (PSS, $M_w \approx 1$ M) and poly(vinyl alcohol) (PVA), are from Sigma-Aldrich. The remaining solvents, 18 MΩ Milli-Q deionized water, chemicals, and laboratory supplies used during film fabrication are acquired from Fisher-Scientific. During experimental validation tests, the films are affixed onto poly(vinyl chloride) PVC Type I plates (McMaster-Carr) using CN-Y post-yield epoxy from Tokyo Kenkyujo, Inc. Conductive electrodes (i.e., 3 M copper tape and conductive silver paste) are acquired from Ted Pella, and stranded wires are from Digi-Key. The PVDF (28-μm thick) films employed for performance comparison tests are from Measurement Specialties, Inc.

Thin film fabrication

Fabrication of the piezoelectric thin films relies on room temperature (25 °C) evaporation of dispersed ZnO nanoparticles (NPs) in polyelectrolyte solutions (Fig. 1). Unlike other nanocomposite fabrication processes that require plasma [23] or high temperatures [20], the approach employed herein is simple, low cost, and straightforward. Before film fabrication, ZnO NPs are mixed with 1.0 wt% PSS solutions at specific concentrations. In order to effectively engage the inherent piezoelectricity of ZnO nanoparticles, dispersion of nanomaterials in solution is crucial. Dispersion is achieved via steric stabilization by subjecting ZnO–PSS solutions to 180 min of bath sonication (135 W, 42 kHz) followed by 30 min of high-energy probe sonication (4.76 mm tip, 150 W, 22.0 kHz), leading to the original mixture to become a uniform, white, ink-like fluid. In contrast, an earlier study conducted by Loh and Chang [24] has already shown that ZnO–PSS mixtures without ultrasonication treatment behave as two-phase mixtures. In this case, the ZnO nanoparticles readily
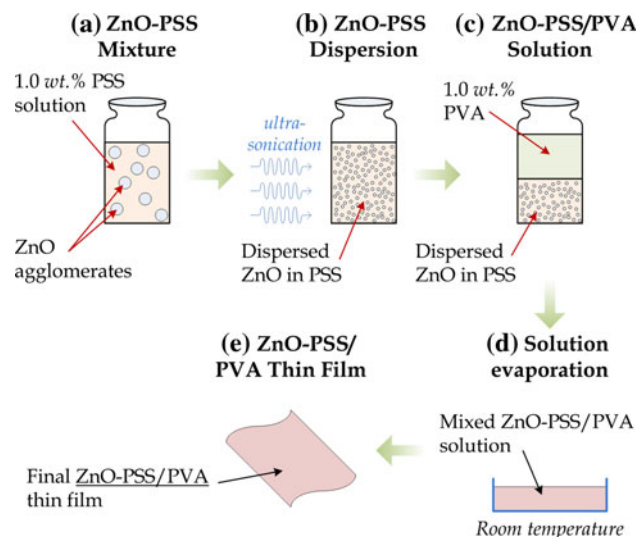
Fig. 1 The schematic illustrates the fabrication of (ZnO–PSS/PVA)$_{wf}$ nanocomposites via a solvent evaporation methodology. Fabrication begins with **a** mixing of ZnO NPs with a PSS solution, **b** steric stabilization dispersion using ultrasonication, and followed by **c** mixing at a 1:1 ratio with a PVA solution. **d** The solvent is evaporated, and **e** the dried film is used as is for testing

agglomerate and precipitate out of solution, and the two-phase mixtures are unsuitable for thin film fabrication, thus highlighting the importance of ZnO dispersion.

Upon dispersion, the ZnO–PSS solution is mixed at a 1:1 ratio with 1.0 wt% PVA solution in a 20-mL scintillation vial (Table 1). Previous preliminary results [25] and previous studies of layer-by-layer polyelectrolyte thin films [26, 27] have indicated that the incorporation of PVA within the polymeric matrix enhances bulk film flexibility and conformability. Then, 5 mL of the ZnO–PSS/PVA solution is poured into a 47-mm Petri dish, and solvent evaporation at 25°C proceeds for approximately 72–96 h. It should be noted that, since the ZnO–PSS/PVA solutions simply expand out in the Petri dishes due to gravity, it is crucial that the Petri dishes are placed on a leveled platform throughout the evaporation process to obtain uniformly thick thin films. Thus, the Petri dishes and thin films

used in this study are cast on a leveled laboratory bench top. The entire fabrication process is also illustrated in Fig. 1.

Finally, the evaporated thin films are carefully peeled off the substrate and used as is for the remainder of this study. The nanocomposites are denoted as (ZnO–PSS/PVA)$_{wf}$, where the subscript wf corresponds to the ZnO weight fraction relative to the bulk film, as can be calculated using Eq. 1:

$$wf = \frac{w_{ZnO}}{w_{ZnO} + w_{PSS} + w_{PVA}} \cdot 100\% \qquad (1)$$

where w is the mass of the raw material (i.e., as indicated by the subscript) used during film fabrication. In total, seven unique thin film sample sets of ZnO weight fractions ranging from 0 to 60% (i.e., in 10% ZnO weight fraction increments) are fabricated for this study and are shown in Table 1. The 0% weight fraction sample set or pristine PSS/PVA films are employed as control specimens.

Mechanical stress–strain testing

The mechanical properties of the (ZnO–PSS/PVA)$_{wf}$ thin films are evaluated via monotonic uniaxial stress–strain tests. Initially, as-fabricated (ZnO–PSS/PVA)$_{wf}$ nanocomposites are cut to approximately 3×45 mm^2 strips to obtain high aspect ratio specimens for minimizing Poisson's effect during tensile testing. The specimens are also cut such that the films have smooth edges so as to prevent pre-mature failure due to stress concentrations and crack initiation/propagation. Then, the specimens are mounted in a TestResources 150R load frame, and the load frame executes a tensile displacement-controlled loading profile at 20 µm s^{-1} load rate (Fig. 2). The applied load and crosshead displacement are sampled at 30 Hz. Upon testing, stress and strain are calculated from the film dimensions, where the specimen length and width are measured using a Neiko digital caliper with 5-µm resolution, and film thickness (typically approximately 50 µm) is measured via a Mitutoyo caliper (1-µm resolution). For each sample set (i.e., unique ZnO weight fraction) shown in Table 1, five to

Table 1 Different weight fraction thin film sample sets and their constituents

Sample set	Weight fraction, wf (%)	Mass of ZnO, w_{ZnO} (mg)	Mass of PSS, w_{PSS} (mg)	Mass of PVA, w_{PVA} (mg)
(ZnO–PSS/PVA)$_{0\%}$	0	0	100.0	100.0
(ZnO–PSS/PVA)$_{10\%}$	10	22.2	100.0	100.0
(ZnO–PSS/PVA)$_{20\%}$	20	50.0	100.0	100.0
(ZnO–PSS/PVA)$_{30\%}$	30	85.7	100.0	100.0
(ZnO–PSS/PVA)$_{40\%}$	40	133.3	100.0	100.0
(ZnO–PSS/PVA)$_{50\%}$	50	200.0	100.0	100.0
(ZnO–PSS/PVA)$_{60\%}$	60	300.0	100.0	100.0

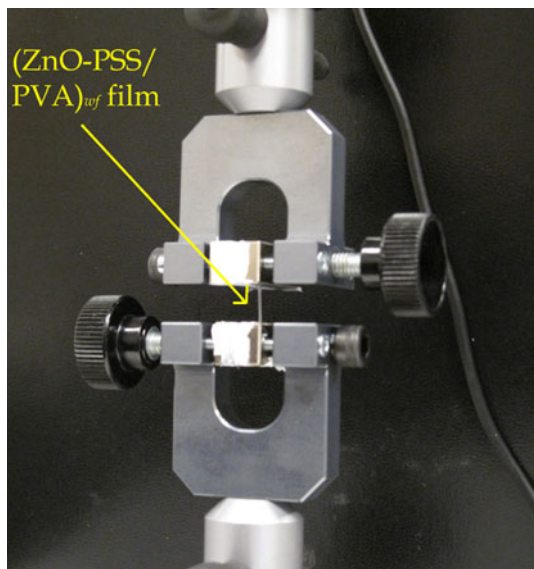**Fig. 2** A TestResources 150R load frame is commanded to apply monotonic uniaxial tensile load to (ZnO–PSS/PVA)$_{wf}$ specimens to determine the thin film stress–strain responses and bulk film mechanical properties

ten specimens are tested for obtaining a good statistical representation of thin film mechanical performance.

Piezoelectric testing specimen preparation

Each specimen from the various (ZnO–PSS/PVA)$_{wf}$ thin film sample sets listed in Table 1 is mechanically etched to approximately 10×10 mm^2 specimens suitable for piezoelectric dynamic strain sensing validation tests. Similar to the aforementioned section, the precise film dimensions and thickness are measured using a Neiko digital caliper and Mitutoyo caliper, respectively. The nanocomposite specimen is then affixed via CN-Y post-yield strain gage epoxy onto the surface at one end of a 30-cm long, 7.6-cm wide, and 0.3-cm thick PVC plate. It should be noted that

the CN-Y epoxy employed is widely used for laboratory and field instrumentation of metal-foil strain gages and enables excellent strain transfer between the substrate and strain sensor (i.e., in this case, the (ZnO–PSS/PVA)$_{wf}$ thin films).

After the epoxy is allowed to dry for 2–3 h, two boundary electrodes are fixed onto the nanocomposite surface to allow for electrical voltage measurements during experimental testing. To establish the electrodes, stranded wire is initially soldered to one end of each conductive copper tape strip. The wire and copper tape are then affixed onto opposite ends of the (ZnO–PSS/PVA)$_{wf}$ thin film as shown in Fig. 3a. In order to minimize contact impedance and to ensure secure bonding during piezoelectric validation and testing, conductive silver paste is painted over the film and copper tape and is left to dry at room temperature for 1 h. The electrode configuration shown in Fig. 3a is similar to that of a two-point probe voltage measurement setup and measures electrical flow in-plane of the film and not through its thickness. The aforementioned procedure is repeated to affix a total of three (ZnO–PSS/PVA)$_{wf}$ thin films of different weight fractions side-by-side on the PVC plate as shown in Fig. 3b. It should be mentioned that the control specimen (i.e., 0% weight fraction PSS/PVA film) is also mounted onto a PVC plate to show that PSS/PVA films without ZnO nanoparticles are not piezoelectric. In addition, a metal-foil strain gage is also mounted alongside the ZnO-based films and connected to a Wheatstone bridge circuit for measuring induced surface strains on the PVC substrate during testing (Fig. 3b).

Piezoelectricity and dynamic strain monitoring characterization

Nanocomposite piezoelectricity and its dynamic strain monitoring capabilities are validated and characterized by measuring the electrical potential generated during free

Fig. 3 **a** The copper tape and silver paste electrodes are mounted to opposite ends of each ZnO–PSS/PVA thin film. **b** Validation of thin film piezoelectricity and strain sensing capabilities is performed by affixing three ZnO-based films and a metal-foil strain gage onto one end of a cantilevered beam. The films' generated voltages and strain gage response are measured with an Agilent MSO8104A oscilloscope during free vibration of the PVC cantilevered beam
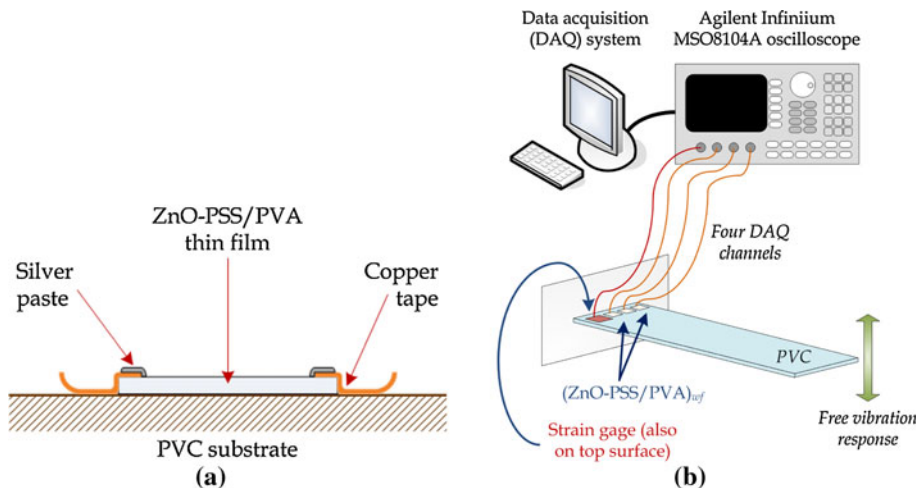
vibration of cantilevered PVC plates. First, the PVC plate specimens described in the previous section are clamped to a laboratory bench top using C-clamps to form a cantilevered beam structure (i.e., the end of the beam where the films are mounted is clamped). Second, an initial displacement is applied to the free end of the beam and released to induce free vibration response; during beam vibration, maximum strain occurs closest to the fixed end where the films and strain gage are mounted. Finally, during free vibration of the PVC plate, a four-channel Agilent Infiniium MSO8104A mixed-signal oscilloscope is employed for measuring thin film generated voltages (Fig. 3b). One of the channels of the oscilloscope is utilized for measuring the voltage output from the Wheatstone bridge circuit and strain gage, while the other three channels measure generated voltages from the (ZnO–PSS/PVA)$_{wf}$ nanocomposites. A series of experiments are conducted so that five to ten (ZnO–PSS/PVA)$_{wf}$ specimens from each thin film sample set in Table 1 are tested.

Piezoelectric performance comparison

In addition to the piezoelectric validation and characterization study, the (ZnO–PSS/PVA)$_{wf}$ thin film's piezoelectricity is also compared to that of commercial PVDF films. Following the procedure outlined in the previous section and in addition to the (ZnO–PSS/PVA)$_{wf}$ film and metal-foil strain gage, PVDF films are also affixed onto the PVC substrates. Similar to the ZnO-based nanocomposites, two boundary electrodes are established via stranded wire, copper tape, and conductive silver paste (Fig. 3a). Then, the PVC beam is clamped at one end to form the cantilevered beam and is subjected to free vibration. During free vibration, an Agilent Infiniium MSO8104A oscilloscope is employed to simultaneously measure the generated

voltages of the ZnO and PVDF films; the voltage output from the Wheatstone bridge and metal-foil strain gage is also recorded.

Results and discussion

Thin film morphology

It has already been demonstrated that ZnO nanomaterials are inherently piezoelectric [17, 18, 28]. However, the objective of this study is to take advantage of ZnO nanoparticle piezoelectricity, scale up their properties, and investigate the effects of nanoparticle weight fractions on bulk film mechanical and piezoelectric performance. Thus, following the aforementioned nanomaterial dispersion and evaporation-based fabrication procedures, seven sample sets of (ZnO–PSS/PVA)$_{wf}$ nanocomposites have been fabricated according to Table 1.

Specimens from each weight fraction sample set are imaged using an FEI 430 NanoSEM scanning electron microscope, and Fig. 4 presents low- and high-magnification SEM images of a (ZnO–PSS/PVA)$_{50\%}$ specimen. From Fig. 4a, it can be observed that ZnO nanoparticles are randomly distributed throughout the entire film's polymeric matrix, thereby suggesting that the material behaves homogeneously at macro-length scales. More importantly, the higher magnification SEM image of Fig. 4b shows that the film is comprised of only individual and small agglomerations of ZnO NPs (i.e., clusters of tens to hundreds of nanoparticles), and the size of individual particles typically range between 20 and 45 nm. Here, the purpose of conducting ZnO particle size measurements using the SEM is not to obtain a statistical nanoparticle size distribution but is rather used for providing a quantitative
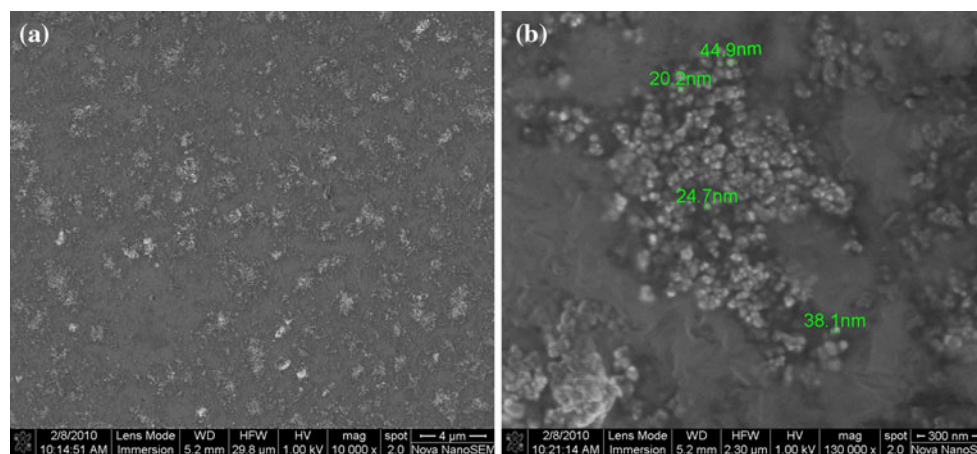

Fig. 4 The **a** low magnification (×10,000) and **b** high-magnification (×130,000) SEM images of a (ZnO–PSS/PVA)$_{50\%}$ thin film show random deposition of individual and small agglomerations (ranging between 20 and 45 nm) of ZnO nanoparticles within the polymeric matrix

estimate of the typical ZnO sizes embedded in the polymeric matrix. Since the pristine ZnO nanoparticles are characterized by an average diameter of 20 nm, Fig. 4b confirms that the sonication process adopted for this study is sufficient to achieve adequate dispersion, and the fabrication methodology employed does not promote significant NP agglomerations. It should also be mentioned that the SEM study conducted has also allowed the authors to identify greater density of nanoparticles associated with increasing ZnO weight fractions.

Nanocomposite mechanical performance

Once the physical properties of the (ZnO–PSS/PVA)$_{wf}$ thin films have been characterized, tensile testing is conducted for investigating how ZnO NPs and their corresponding weight fractions influence bulk nanocomposite mechanical performance. Monotonic uniaxial tensile tests are conducted, and Fig. 5 plots an overlay of representative stress–strain diagrams for (ZnO–PSS/PVA)$_{20\%}$ to (ZnO–PSS/PVA)$_{50\%}$ thin films. From the stress–strain diagrams shown in Fig. 5, it can be immediately observed that ZnO weight fraction significantly affects nanocomposite stress–strain response and their corresponding mechanical properties. While all films exhibit an initial linear stress–strain region, low weight fraction films show greater flexibility, whereas high weight fraction films exhibit sudden and brittle fracture failure at low levels of applied strain.

In particular, the film's modulus of elasticity (E), ultimate strength (σ_f), and ultimate failure strain (ε_f) is determined from the experimental stress–strain responses. Figure 6 and Table 2 show how ZnO weight fraction

influences the aforementioned bulk film mechanical properties being investigated in this study. In a previous study by Loh et al. [27], the mechanical properties of pristine PSS/PVA thin films have been determined via stress–strain testing, and the results are also included for comparison in Fig. 6 and Table 2. From Fig. 6a, it can be seen that with more ZnO NPs embedded within the nanocomposite matrix, the film becomes stiffer; the film's average Young's modulus increases from 340 MPa for 0% ZnO weight fraction to as high as 1,080 MPa for 50% ZnO weight fraction. This response is expected since the flexible polymeric matrix is being filled with more and more stiffer particles as weight fraction increases. However, associated with the increase in ZnO weight fraction (and increase in modulus of elasticity) is the simultaneous decrease in bulk film ultimate failure strain (Fig. 6c). The nanocomposite becomes more brittle due to ZnO nanoparticles serving as defect sites that promote stress concentrations, crack initiation, and ultimately fracture failure of the thin film.

Finally, it can be observed from Fig. 6b that 20 and 30% ZnO weight fraction films exhibit the highest ultimate strength. It can also be seen from Fig. 6b and Table 2 that the average ultimate strength for 10% ZnO weight fraction films is approximately 11.3 MPa. It is hypothesized that the true average ultimate strength of (ZnO–PSS/PVA)$_{10\%}$ films should be closer to 20–25 MPa according to the results and trend shown in Fig. 6c. It is possible that experimental error or defective films may have caused this potentially erroneous data point. Otherwise, the results
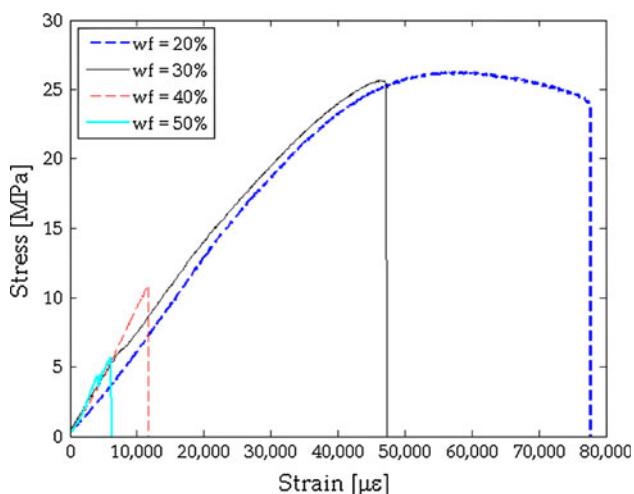
Fig. 5 The overlay of 20 to 50% ZnO weight fraction thin film stress–strain responses show that these nanocomposites are characterized by an initial linear region followed by potential yielding and fracture failure. The stress–strain response is dependent on zinc oxide weight fraction
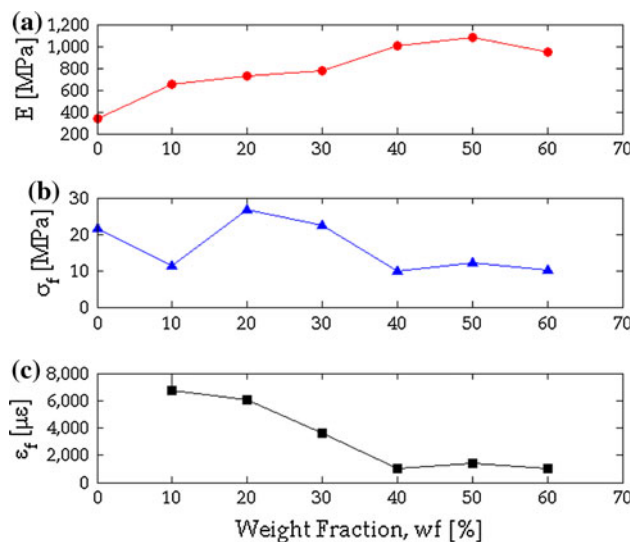
Fig. 6 The stress–strain responses from every specimen of various weight fraction sample sets are analyzed, and the average **a** modulus of elasticity, **b** ultimate strength, and **c** ultimate failure strain are plotted as a function of ZnO weight fraction. It should be noted that at 0% weight fraction, the pristine PSS/PVA film fails at approximately 250% or 2,500,000 μɛ. This data point is not shown in **c** so as to better visualize the remaining ultimate failure strain data corresponding to different ZnO weight fractions

Table 2 Summary of thin film mechanical properties determined from stress–strain testing

Sample set	Average nanocomposite mechanical properties		
	Modulus of elasticity, E (MPa)	Ultimate tensile strength, σ_f (MPa)	Ultimate failure strain, ε_f (μɛ)
$(ZnO–PSS/PVA)_{0\%}^{a}$	340	21.7	2,500,000
$(ZnO–PSS/PVA)_{10\%}$	655	11.3	6,780
$(ZnO–PSS/PVA)_{20\%}$	724	26.8	6,060
$(ZnO–PSS/PVA)_{30\%}$	780	22.3	3,610
$(ZnO–PSS/PVA)_{40\%}$	1,010	9.8	1,000
$(ZnO–PSS/PVA)_{50\%}$	1,080	12.2	1,390
$(ZnO–PSS/PVA)_{60\%}$	949	10.1	1,050

[a] These results have been obtained from a separate study and are included for comparison purposes

shown in Fig. 6c suggest that the average ultimate strength becomes compromised with excess amounts of ZnO nanoparticles embedded in the polymeric matrix.

Of equal importance is how the ZnO-based films' mechanical properties compare to those of other piezoelectric polymer films. Overall, the results obtained in Fig. 6 suggest that the ZnO-based nanocomposites are characterized by lower modulus of elasticity and ultimate strength as compared to PVDF films. Vinogradov and Holloway [29] has shown that the average Young's modulus and ultimate strength of PVDF films (i.e., in the direction parallel to PVDF molecular chains) are approximately 2.7 GPa and 350 MPa, respectively. Thus, although $(ZnO–PSS/PVA)_{wf}$ films do not possess high strength, they are less stiff and can easily conform to various structural shapes.

Piezoelectricity and dynamic strain monitoring characterization

The cantilevered beam free vibration tests are conducted to characterize $(ZnO–PSS/PVA)_{wf}$ thin film piezoelectricity. Characterization and comparison of piezoelectric performance can be achieved by comparing thin film generated voltages in response to applied dynamic strain (i.e., $\partial\varepsilon/\partial t$ or $\Delta\varepsilon/\Delta t$ due to the induced surface strains during free vibration). For the same magnitude of applied dynamic strain, thin film generated voltages are correlated to its piezoelectricity and dimensions. While all of the nanocomposite specimens are cut to approximately 10×10 mm^2, film dimensions and nanocomposite thickness can still vary between different specimens and sample sets. Thus, Eq. 2 is employed for normalizing output voltages with the precise and accurate film dimension measurements to provide for an accurate comparison:

$$V_{\text{Norm}} = \frac{V_{\text{Out}} \cdot l}{w \cdot t} \qquad (2)$$

where V_{Out} is the thin film output voltage, l is the distance between the two electrodes (or gage length), w is the width of the film, and t is the thickness.

First, the free vibration tests conducted on the 0% weight fraction or pristine PSS/PVA thin films did not produce any significant generated voltages or piezoelectric response exceeding the sensor noise floor. This result confirms that PSS/PVA films do not possess inherent piezoelectricity. On the other hand, Figs. 7a and 8a show representative overlays of $(ZnO–PSS/PVA)_{50\%}$ and $(ZnO–PSS/PVA)_{60\%}$ normalized generated voltages in response to dynamic strain due to free vibration of the PVC beam. More specifically, nanocomposite generated voltages increase in tandem with increasing dynamic strain (and the opposite is true during the compression cycle). These results confirm the piezoelectricity of $(ZnO–PSS/PVA)_{wf}$ films such that the films generate voltage in response to dynamic strains. In addition, since pristine PSS/PVA films are not piezoelectric, it can be concluded that the $(ZnO–PSS/PVA)_{wf}$ films derive their piezoelectricity from the embedded nanoparticles.

However, it can also be observed from Figs. 7a and 8a that the ZnO-based films are characterized by a higher noise floor (i.e., typically on the order of ±0.01 mV cm^{-1}) as compared to the dynamic strain measurements. Since the ZnO nanocomposites are mounted with simple copper tape and silver paste electrodes, it is likely that the elevated noise floor is caused by the lower quality electrodes. In addition, since the Agilent Infiniium MSO8104A mixed-signal oscilloscope employed for voltage measurements is a high resolution device and that the measured voltages are typically in the range of 10–100 mV, noise is likely due to the electrodes and not the measuring equipment. Thus, reduction of the noise floor in future studies can be achieved by improving the quality of the conducting electrodes or by incorporating a low-pass filter. Nevertheless, these results suggest that the nanocomposites fabricated in this study have the potential for dynamic strain monitoring. It should be mentioned that the ZnO-based films have only been shown to generate voltage in response to changes in applied dynamic strain but not static strain.

To further characterize their piezoelectric and dynamic strain sensing performance, the results from the free vibration tests can be plotted differently to show
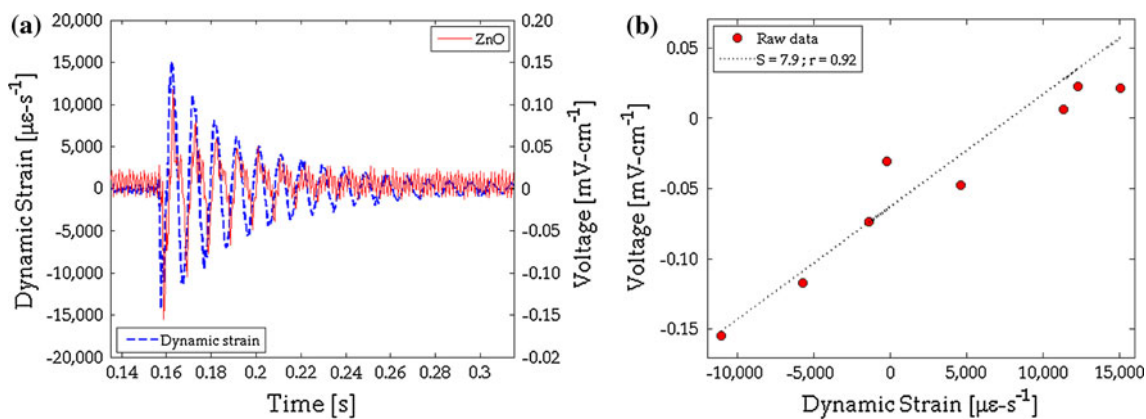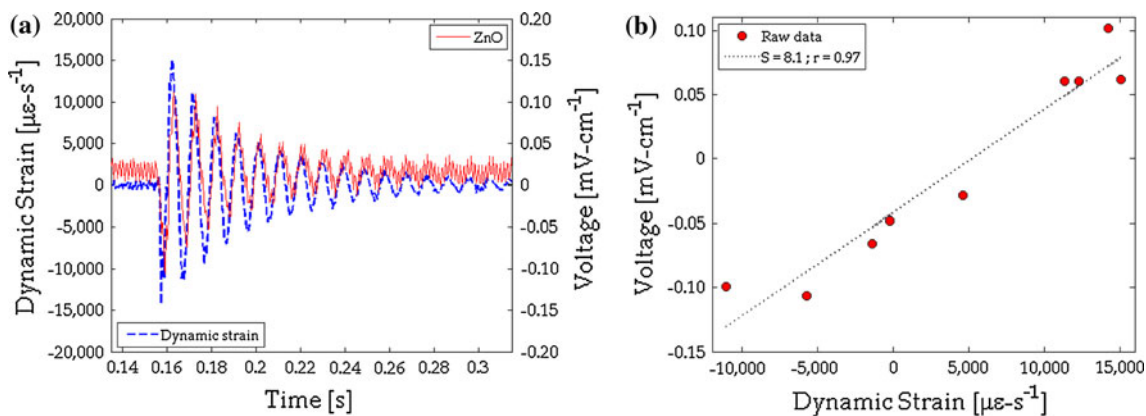
Fig. 7 Free vibration testing of the cantilevered beam is conducted, and **a** the generated voltage time history response of a representative (ZnO–PSS/PVA)$_{50\%}$ thin film is overlaid with the induced dynamic strain (as measured by the metal-foil strain gage). **b** The corresponding film's normalized voltage response is plotted as a function of dynamic strain, and the strain sensitivity of the film is approximately 7.9 mV s $\mu\varepsilon^{-1}$ cm^{-1}

Fig. 8 Free vibration testing of the cantilevered beam is conducted, and **a** the generated voltage time history response of a representative (ZnO–PSS/PVA)$_{60\%}$ thin film is overlaid with the induced dynamic strain (as measured by the metal-foil strain gage). **b** The corresponding film's normalized voltage response is plotted as a function of dynamic strain, and the strain sensitivity of the film is approximately 8.1 mV s $\mu\varepsilon^{-1}$ cm^{-1}

normalized generated voltages (Eq. 2) as a function of induced dynamic strain (Figs. 7b, 8b). Only the data from the first vibration cycle is included in Figs. 7b and 8b. Regardless, the results show that normalized generated voltages vary near-linearly with dynamic strain. In fact, a linear least-squares regression line can be fitted to the experimental data. The sensor's dynamic strain sensitivity (*S*) is equivalent to the slope of the least-squares fitted line and can be calculated using Eq. 3:

$$S = \frac{V_{\text{Norm}}}{\Delta\varepsilon/\Delta t} \qquad (3)$$

where $\Delta\varepsilon/\Delta t$ is the induced dynamic strain calculated using discrete strain measurements obtained from a traditional metal-foil strain gage affixed onto the PVC beam surface.

The linear least-squares regression analysis is performed on all the free vibration experimental data (i.e., for five to ten specimens per ZnO weight fraction sample set of

Table 1). The average dynamic strain sensitivities and their corresponding error bars (i.e., using the standard deviation) are tabulated in Table 3 and also illustrated in Fig. 9. From Fig. 9, it can be clearly observed that the nanocomposite's average dynamic strain sensitivity increases near-linearly with ZnO weight fraction. These results suggest that one can begin to tune the film's dynamic strain sensitivity by simply varying the amount of ZnO NPs embedded during fabrication. The results shown in Fig. 9 are also expected, since with greater amounts of ZnO within the composite matrix, more ZnO nanoparticles are available to contribute their inherent piezoelectricity to the entire film. In this study, the highest dynamic strain sensitivity achieved is 9.7 mV s $\mu\varepsilon^{-1}$ cm^{-1} and is for a (ZnO–PSS/PVA)$_{60\%}$ film, and it is still possible to increase strain sensitivity by employing even higher weight fraction films. However, one can also observe that the variation in dynamic strain sensitivity also increases with increasing weight fraction.

Table 3 Summary of thin film dynamic strain sensitivities determined from free vibration testing

Sample set	Dynamic strain sensitivity, S (mV s $\mu\varepsilon^{-1}$ cm^{-1})	Error or standard deviation (mV s $\mu\varepsilon^{-1}$ cm^{-1})
(ZnO–PSS/PVA)$_{0\%}$	0	0
(ZnO–PSS/PVA)$_{10\%}$	1.02	0.28
(ZnO–PSS/PVA)$_{20\%}$	2.08	0.05
(ZnO–PSS/PVA)$_{30\%}$	2.38	0.61
(ZnO–PSS/PVA)$_{40\%}$	4.02	1.99
(ZnO–PSS/PVA)$_{50\%}$	5.70	1.43
(ZnO–PSS/PVA)$_{60\%}$	6.64	2.09
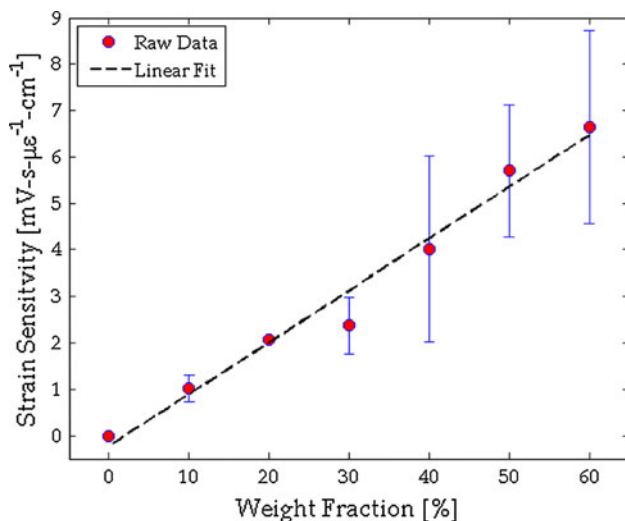
Fig. 9 The average dynamic strain sensitivity for each of the (ZnO–PSS/PVA)$_{wf}$ thin film sample set is computed, and their corresponding error bars (i.e., one standard deviation) are also shown

The greater variation at higher concentrations may be due to decreased homogeneity and selective nanoparticle agglomerations, thereby suggesting that there is a limit as to how much ZnO NPs can be embedded within the thin film architecture.

Piezoelectric performance comparison

Lastly, the piezoelectric performance of (ZnO–PSS/PVA)$_{wf}$ nanocomposites is compared to that of commercial PVDF thin films as have been outlined earlier. Figure 10 plots an overlay of the as-measured generated voltage for (ZnO–PSS/PVA)$_{60\%}$ and PVDF films during free vibration response of a cantilevered PVC beam. From the results shown in Fig. 10, it can be concluded that (ZnO–PSS/PVA)$_{60\%}$ thin films exhibit comparable, if not better, piezoelectricity than commercially available PVDF films. After the beam has stopped vibrating (i.e., after about
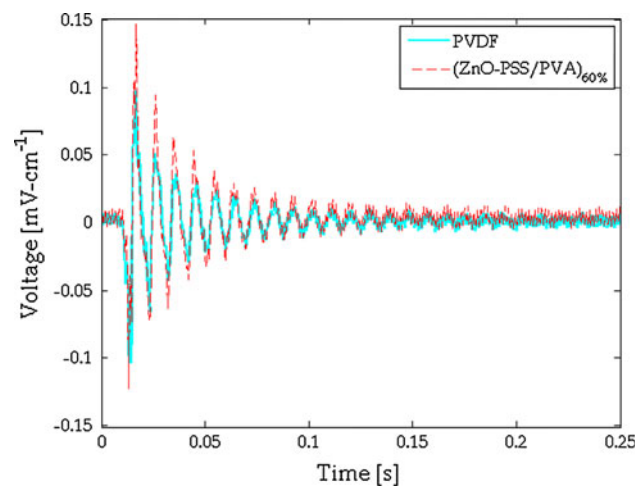
Fig. 10 The normalized generated voltages of (ZnO–PSS/PVA)$_{60\%}$ and commercial PVDF thin film are overlaid to compare their piezoelectric and dynamic strain sensing performance

0.15 s in Fig. 10), the two films are characterized by comparable noise floors. It should also be noted that 50% weight fraction films also exhibit comparable performance attributes; however, lower weight fraction films generate less voltage as compared to PVDF thin films. In addition, commercial PVDF thin films are subjected to high-voltage corona poling and cyclic stretching for aligning PVDF molecules and for enhancing their remnant piezoelectricity [5]. In contrast, the nanocomposites employed in this study are not subjected to the aforementioned high-voltage poling and post-fabrication treatment processes. However, it is hypothesized that moderate poling can further enhance nanocomposite piezoresistivity and dynamic strain sensing sensitivity, but further research and additional testing are required to confirm this hypothesis.

Conclusions

In summary, the objective of this study is to investigate the mechanical and piezoelectric performance of (ZnO–PSS/PVA)$_{wf}$ nanocomposites for dynamic strain sensing. A total of seven unique sets of thin films with different ZnO nanoparticle weight fractions have been fabricated via an evaporation technique. First, specimens from each sample set are subjected to monotonic uniaxial tensile testing to investigate their stress–strain response. The stress–strain diagrams suggest that the films are characterized by an initial linear region, and some films of low ZnO weight fractions can exhibit slight yielding followed by fracture failure. It has also been shown that even though the bulk nanocomposite stiffness (or modulus of elasticity) increases with increasing ZnO weight fractions, there is a tradeoff since the material becomes more brittle (i.e., decreased

ultimate failure strain). On the other hand, when compared to PVDF, ZnO nanocomposites are characterized by lower modulus of elasticity and ultimate strength regardless of ZnO weight fraction.

The second major portion of this study has focused on characterizing the piezoelectric performance of the proposed ZnO-based nanocomposites. It has been confirmed through free vibration cantilevered beam tests that the $(ZnO–PSS/PVA)_{wf}$ films are in fact piezoelectric and generate voltage in response to dynamic strain of the substrate. More importantly, one can begin to tune the piezoelectricity of the film by controlling the film's ZnO weight fraction. The experimental results suggest that increasing ZnO weight fraction leads to a near-linear increase in their dynamic strain sensitivity and piezoelectricity. The piezoelectric and dynamic strain sensing performance of the ZnO-based films are also compared to that of commercial PVDF thin films. It has been found that 50 and 60% films exhibit comparable dynamic strain sensitivity and piezoelectricity while not requiring high-voltage poling and mechanical stretching as do PVDF-based films.

While this preliminary study has only focused on exploring the relationship between ZnO weight fraction and bulk film mechanical performance and piezoelectricity, other factors may also be used and explored for improving their performance. For instance, it is hypothesized that high-voltage poling applied to $(ZnO–PSS/PVA)_{wf}$ thin films can further improve their piezoelectricity, and further research is currently underway to explore this idea. On the other hand, future testing will also investigate the effects of film thickness. Other studies related to carbon nanotube-based thin films have shown that increasing nanocomposite thickness can decrease strain sensitivity while improving mechanical performance [30]. It is possible that the mechanical properties of ZnO-based film will improve with increasing film thickness since the nanocomposites will become less sensitive to thin film inhomogeneity due to nanoparticle agglomerations and stress concentrations.

References

1. Park S, Yun C-B, Inman DJ (2008) Fatigue Fract Eng Mater Struct 31(8):714
2. Yu L, Santoni-Bottai G, Xu B, Liu W, Giurgiutiu V (2008) Fatigue Fract Eng Mater Struct 31(8):611
3. Moheimani SOR, Fleming AJ (2006) Piezoelectric transducers for vibration control and damping, edn. Springer, Germany
4. Sodano HA, Inman DJ, Park G (2004) Shock Vib Dig 36(3):197
5. Wang TT, Herbert JM, Glass AM (eds) (1988) The applications of ferroelectric polymers. Blackie and Son Ltd, London
6. Stein PK (2006) Exp Tech 30:23
7. Kersey AD (1996) Opt Fiber Technol 2(3):291
8. Lynch JP, Loh KJ (2006) Shock Vib Dig 38(2):91
9. Beeby S, Ensell G, Kraft M, White N (2004) Mems mechanical sensors, edn. Artech House, Norwood
10. Polla DL, Francis LF (1998) Annu Rev Mater Sci 28(1):563
11. Jiansirisomboon S, Songsiri K, Watcharapasorn A, Tunkasiri T (2006) Curr Appl Phys 6(3):299
12. Shotton KC, Bacon DR, Quilliam RM (1980) Ultrasonics 18(3):123
13. Takeno A, Okui N, Kitoh T, Muraoka M, Umemoto S, Sakai T (1991) Electron Opt 202:205
14. Zhang Q-Q, Chan HL-W, Zhou Q, Choy C-L (1999) Mater Res Innov 2(5):283
15. Laxminarayana K, Jalili N (2005) Text Res J 75(9):670
16. Windmill JFC, Zorab Z, Bedwell DJ, Robert D (2008) Nanotechnology 19(3):035506/035501
17. Wang ZL, Song J (2006) Science 312(5771):242
18. Zhu R, Wang D, Xiang S, Zhou Z, Ye X (2008) Nanotechnology 19(28):285712/285711
19. Scrymgeour DA, Sounart TL, Simmons NC, Hsu JWP (2007) J Appl Phys 101(1):014316/014311
20. Lin H-B, Cao M-S, Zhao Q-L, Shi X-L, Wang D-W, Wang F-C (2008) Scr Mater 59(7):780
21. Ji LW, Shih WS, Wu CZ, Peng SM, Meen TH (2010) J Mater Sci 45(12):3266. doi:10.1007/s10853-010-4336-4
22. Gowri VS, Almeida L, Amorim MTPD, Pacheco NC, Souto AP, Esteves MF, Sanghi SK (2010) J Mater Sci 45(9):2427. doi:10.1007/s10853-010-4210-4
23. Bdikin IK, Gracio J, Ayouchi R, Schwarz R, Kholkin AL (2010) Nanotechnology 21(23):235703/235701
24. Loh KJ, Chang D (2009) In: Proceedings of 7th international workshop on structural health monitoring, vol 2, Stanford, pp 1774–1781
25. Chang D, Loh KJ (2010) In: Proceedings of 5th international conference on bridge maintenance, safety and management, Philadelphia, 12–15 July 2010
26. Loh KJ, Kim J, Lynch JP, Kam NWS, Kotov NA (2007) Smart Mater Struct 16(2):429
27. Loh KJ, Thouless M, Lynch JP (2009) In: Proceedings of 12th international conference on fracture, Ottawa, 12–17 July 2009
28. Wang M-R, Wang J, Chen W, Wang L-D (2005) J Mater Sci 40(19):5281. doi:10.1007/s10853-005-0520-3
29. Vinogradov A, Holloway F (1999) Ferroelectrics 226(1):169
30. Loh KJ, Lynch JP, Shim BS, Kotov NA (2008) J Intell Mater Syst Struct 19(7):747